applied sciences

MDPI

Article

The Concentration Effect of Acetone on the Kinetics of Alkaline Water Electrolysis Studied on Selected 3D Nickel Catalysts

Julia Kwiatkowska and Bogusław Pierożyński *

Department of Chemistry, Faculty of Agriculture and Forestry, University of Warmia and Mazury in Olsztyn, Łódzki Square 4, 10-727 Olsztyn, Poland; julia.kwiatkowska.5@student.uwm.edu.pl
* Correspondence: boguslaw.pierozynski@uwm.edu.pl or bogpierozynski@yahoo.ca

Abstract

This study investigates the impact of acetone on the electrochemical behaviour of 3D nickel foam electrodes in 0.1 M NaOH solution, with respect to the kinetics of alkaline water electrolysis (hydrogen and oxygen evolution reactions: HER and OER, respectively). Cyclic voltammetry (CV), electrochemical impedance spectroscopy (EIS) and Tafel polarisation techniques were employed to investigate the kinetics of these processes for $(CH_3)_2C{=}O$ concentrations ranging from 1.0×10^{-5} to 0.1 M. The fundamental conclusions of this work are related to the fact that acetone, at moderate concentrations, was found to significantly facilitate the kinetics of both the HER and the OER processes, when examined on unmodified Ni foam electrodes. Conversely, the presence of acetone in working electrolyte for a Ru-activated nickel foam electrode resulted in a radical inhibition of the HER kinetics. The above is strongly believed to be associated with an electrode surface poisoning effect, in relation to the Ru sites' blockage by an extensive, flat/side-on coordination of adsorbed acetone molecules. Interestingly, in the presence of Ru, acetone had practically no effect on the recorded OER rates. The above indicates that some organic additives (e.g., acetone) might exhibit significant, although strongly catalyst-dependent, opportunities for facilitation of the industrial alkaline water electrolysis process.

Keywords: acetone; alkaline water electrolysis; AWE; HER; OER

1. Introduction

Alkaline water electrolysis is still an essential process for the production of green hydrogen through employment of renewable energy sources (RES). 3D-type nickel-based catalyst materials are broadly utilised in alkaline water electrolysis, because of their superior electrocatalytic properties, large electrochemically available surface area and chemical resistance under alkaline working conditions [1–3]. Furthermore, it is well-established that introducing various organic additives into the electrolyte could significantly alter the kinetics of both cathodic hydrogen evolution reaction (HER) and anodic oxygen evolution reaction (OER). A number of organic molecules that might be present in the electrolyte—for example, alcohols, ketones and acids—might become electro (sorbed) on the catalyst surface, followed by potential-dependent electro-reduction or/and electro-oxidation processes, hence possibly affecting the kinetics of the process of alkaline water electrolysis [4,5]. In fact, knowing how to choose and apply organic electrolyte additives could considerably accelerate the HER rates, resulting in substantially improved performance of the green hydrogen production via alkaline water electrolysis.

Academic Editors: Michael J. Wagner and Francis Verpoort

Received: 16 May 2026
Revised: 30 June 2026
Accepted: 13 July 2026
Published: 20 July 2026

Interestingly, acetone was found to significantly decrease electrolyte surface tension through reinforced hydrogen bonding when combined with water molecules [6–8]. Furthermore, numerous scientific examinations (under both acidic and alkaline conditions) have shown that acetone and other aliphatic ketones are prone to undergo electrosorption and electrochemical reduction to alcohols when studied on polycrystalline and various Pt single-crystal plane electrodes [9–14].

This article extends from earlier works published from this laboratory on the influence of acetone on the kinetics of alkaline water electrolysis, examined on bulk polycrystalline Ni [15] and Pt [16] electrodes. In both cases (on polycrystalline Ni and Pt electrodes), acetone was found to significantly enhance the HER and OER rates, as compared to those recorded in unmodified 0.1 M NaOH solution. The above was explained in terms of a radical reduction in the electrolyte surface tension parameter, which then enabled the facilitation of hydrogen (and oxygen) bubble detachment from the catalyst surface.

Here, the authors studied the effect of increasing the acetone concentration in 0.1 M NaOH solution on the electrochemical HER and OER characteristics, but also on complex 3D nickel foam and Ru-activated Ni foam electrodes, where acetone adsorption configuration at Ru is fundamentally different from that at Pt (see Section 3.2.1 and Scheme 1). Performed measurements included: cyclic voltammetry (CV), Tafel polarizations (both cathodic and anodic directions), and electrochemical impedance spectroscopy (EIS) examinations.

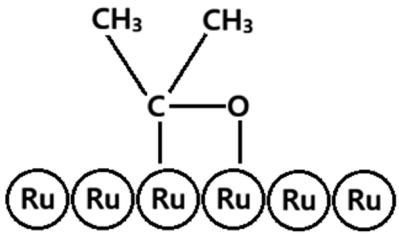

Scheme 1. The proposed flat geometry adsorption scheme of acetone molecule at the Ru surface.

2. Materials and Methods

Ultrapure H_2O delivered by a Millipore Direct-Q3 UV water purification system with 18.2 MΩ cm water resistivity and superior quality NaOH pellets from Merck (Poznań, Poland) were used to make 0.1 M sodium hydroxide electrolyte. The concentration of acetone (Merck, >99%, ACS Reagent, Poznań, Poland) in the working solution covered a range from 1.0×10^{-5} to 0.1 M.

Electrochemical experiments were performed by means of a pyrex-glass cell in a three-electrode configuration, consisting of nickel foam/Ru-activated Ni foam (MTI Corporation, Richmond, CA, USA, purity: >99.99%, thickness 1.6 mm), where the size of Ni foam samples was (9–12) × (10–14) mm and their weight was within the range 35 to 65 mg] working electrodes (WE), a reversible hydrogen electrode (RHE) (HydroFlex®, Biologic, Seyssinet-Pariset, France) as a reference electrode and a coiled Pt wire as a counter electrode (CE). The counter electrode was prepared from 1.0 mm diameter, 99.9998% purity Pt wire, provided by Johnson Matthey, Inc. (Chicago, IL, USA). Spontaneous deposition of Ru on nickel foam samples was conducted in 0.001 M $RuCl_3$ (Sigma-Aldrich, 99.98%, Poznań, Poland) solution at room temperature and pH= 1.5, to produce the catalyst deposits containing below 1 wt.% Ru. Other important details were as previously reported, e.g., in Reference [3] from this laboratory.

Electrochemical experiments were conducted at room temperature and over the temperature range 20–40 °C with the Solartron 12,608 W Full Electrochemical System, comprising 1260 Frequency Response Analyzer (FRA) and 1287 Electrochemical Interface (EI) (AMETEK, Leicester, UK). The cyclic voltammetry trials were performed at a sweep rate of

50 mV s^{-1}, whereas quasi-potentiostatic cathodic (and anodic) Tafel polarisation experiments were recorded at a scan-rate of 0.5 mV s^{-1} at all working electrodes. On the other hand, electrochemical impedance spectroscopy plots were recorded for the frequency range 100 kHz–0.1 Hz (or 1.0 Hz) with an output *ac.* signal set at 5 mV (rms). The instruments were operated by ZPlot 3.6a or Corrware 3.6a software for Windows (Scribner Associates, Inc., Southern Pines, NC, USA). The impedance experiments were carried out in three autonomous tests at each electrode potential value, where the replicability of such recorded impedance results was usually around 10% or less. Then, data analysis was conducted by means of ZView 4.1b or CView 3.6a software package for Windows, where the impedance spectra were fitted with LEVM 6, a complex, non-linear, least-squares immittance fitting program [17].

3. Results

3.1. Cyclic Voltammetry

The cyclic voltammetry behaviour of nickel foam and Ru-modified Ni foam electrodes in 0.1 M sodium hydroxide solution, over the potential range 0.1 to 1.5 or 1.7 V/RHE, in both the absence and presence of acetone (for $(CH_3)_2C{=}O$ concentrations of 1.0×10^{-5}, 1.0×10^{-3} and 0.1 M) is shown in Figures 1 and 2 below. Hence, an anodic peak (observed at ca. 1.30–1.45 V vs. RHE) denotes the creation of β-NiOOH species from nickel hydroxide, which then produces a corresponding cathodic peak, centred at about 1.25 V in relation to the reduction in the formerly produced β-NiOOH [15,18,19].

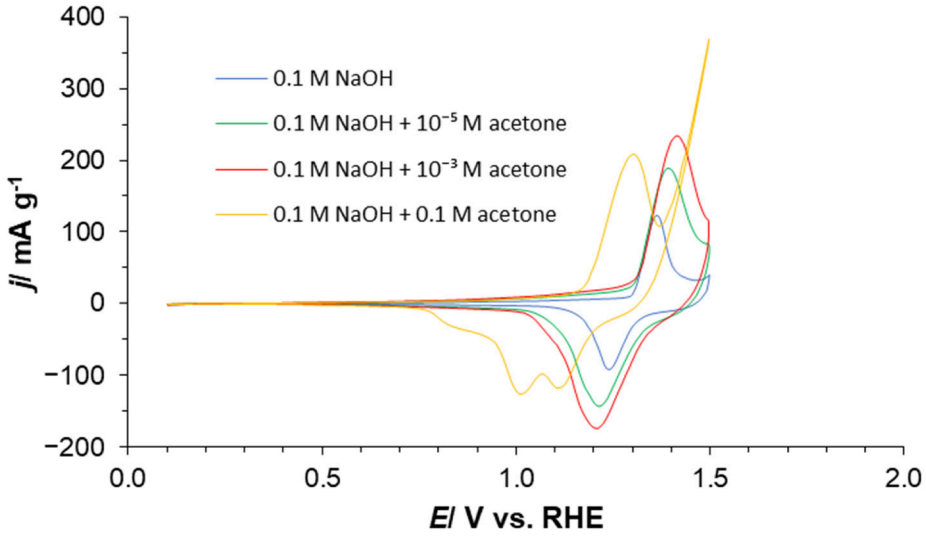

Figure 1. Room-temperature cyclic voltammetry curves (third scan) at the nickel foam working electrode. Voltammetric profiles illustrate the electrochemical response in a blank 0.1 M NaOH background electrolyte, compared to solutions containing 1.0×10^{-5} M, 1.0×10^{-3} M and 0.1 M acetone.

It can be seen in Figure 1 that the introduction of acetone into the working solution results in significantly rising voltammetric cathodic and anodic charges (as well as the respective shifts in the peaks' centres towards lower and higher electrode potentials, respectively) for initial and intermediate acetone concentrations. Conversely, at the highest concentration of acetone (0.1 M), not only the shift in the voltammetric peaks is radical, but also a sharp and large Faradaic current-density appears as a new voltammetric feature, beyond the electrode potential of 1.4 V (significant enhancement of the OER process). This observed behaviour can generally be attributed to being parallel with the formation of nickel oxyhydroxide species, partial surface adsorption of acetone molecules and their electrochemical degradation/fragmentation (proceeding through NiOOH species) to produce,

e.g., acetate (CH_3COO^-) and formate ($HCOO^-$) ions. Furthermore, radical intensification of the OER in the presence of 0.1 M acetone (Figure 1) is strongly believed to be related to the reduction in surface tension of the electrolyte, due to acetone–water hydrogen bonding interactions, leading to the facilitation of the O_2 gas bubbles' surface detachment process.

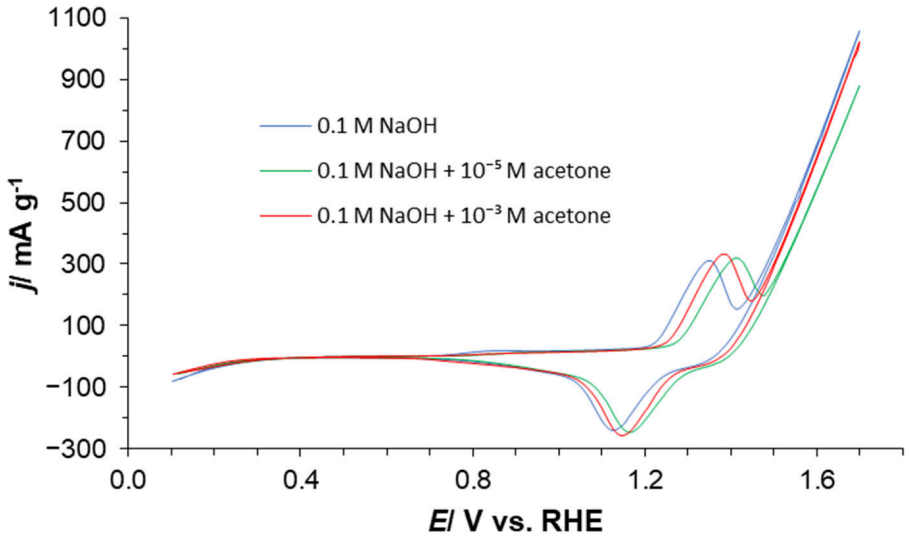

Figure 2. Room-temperature cyclic voltammetry curves (third scan) at the Ru-activated nickel foam working electrode. Voltammetric profiles illustrate the electrochemical response in a blank 0.1 M NaOH background electrolyte, compared to solutions containing 1.0×10^{-5} M and 1.0×10^{-3} M acetone.

On the other hand, the cyclic voltammetric behaviour of the Ru-activated Ni foam composite electrode is presented in Figure 2. Here, the voltammetric changes induced by the presence of acetone are much less significant than those exhibited by the unmodified nickel foam electrode. They are primarily limited to the shifts in the voltammetric current-density maxima (observed over the potential range 1.0–1.6 V/RHE) and displacement of the OER onset towards less anodic potentials (below 1.5 V for acetone concentrations of 1.0×10^{-5} and 1.0×10^{-3} M). This behaviour could be envisaged with severely obstructed adsorption of acetone molecules on ruthenium oxide sites (the predominant adsorption sites on the ruthenium-activated Ni foam electrode), which leads to the kinetics of the oxygen evolution reaction being principally unaffected (Figure 2, compare CV profiles marked in blue and red).

3.2. Ac. Impedance Spectroscopy Behaviour

3.2.1. Hydrogen Evolution Reaction

Ac. impedance behaviour of the process of hydrogen evolution reaction on the unmodified and the Ru-activated nickel foam electrodes in 0.1 M sodium hydroxide supporting solution, in both the absence and presence of acetone (for the concentrations of 1.0×10^{-5}, 1.0×10^{-3} and 0.1 M), is presented in Figures 3–5 and Tables 1–4. Hence, the electrochemical impedance curves for an initial Ni foam electrode exhibited single and slightly depressed semicircles (coherent with a single-step charge-transfer reaction) at all examined electrode potentials, in the explored frequency range (examples of Nyquist impedance plots registered at an overpotential of 200 mV are shown in Figure 3). The overpotential dependence of Faradaic reaction resistance (R_{ct}) and double-layer capacitance (C_{dl}) parameters for the process of HER at the unmodified nickel foam electrode (stemmed from a constant phase element—the CPE-modified Randles equivalent circuit presented in Figure 5) is shown in Table 1. The CPE element was employed in order to account for the so-called

"capacitance dispersion" [20,21] effect, characterised by depressed semicircles within the Nyquist impedance spectra.

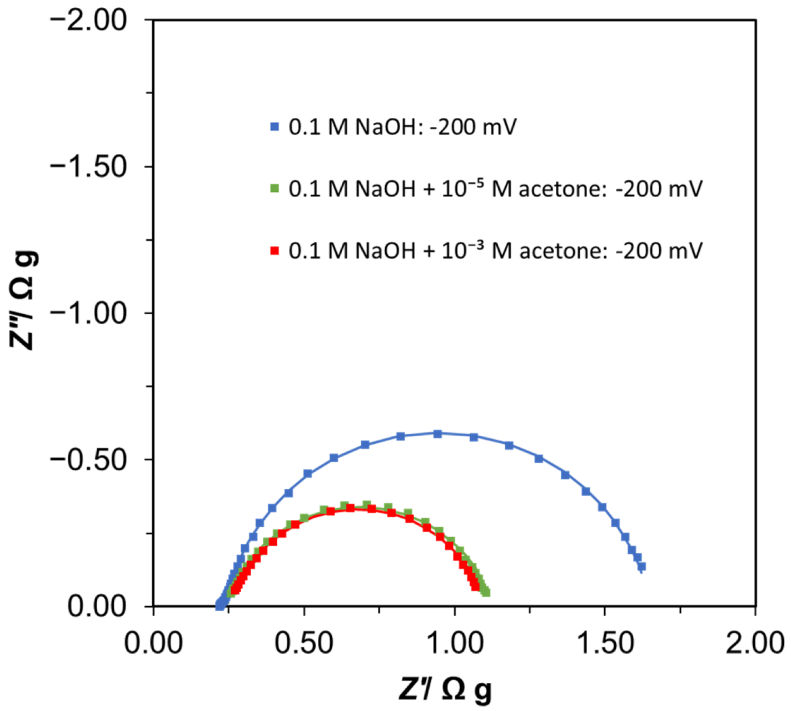

Figure 3. Impedance spectroscopy response (Nyquist curves) of the nickel foam working electrode during the hydrogen evolution reaction. Data were gathered at a constant potential of −200 mV in a blank 0.1 M NaOH background electrolyte, compared to solutions containing 1.0×10^{-5} M and 1.0×10^{-3} M acetone.

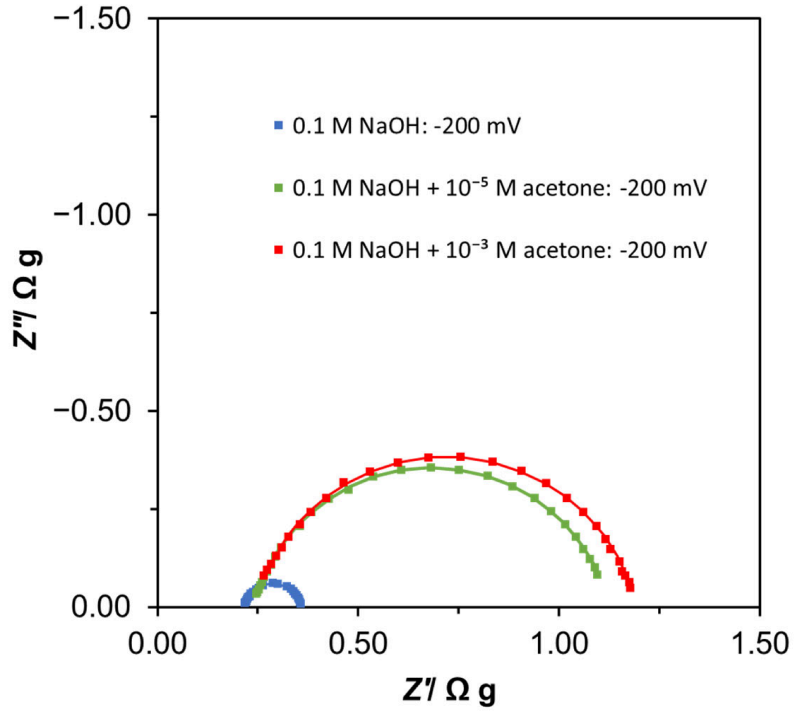

Figure 4. Impedance spectroscopy response (Nyquist curves) of the Ru-activated nickel foam working electrode during the hydrogen evolution reaction. Data were gathered at a constant potential of −200 mV in a blank 0.1 M NaOH background electrolyte and compared to solutions containing 1.0×10^{-5} M and 1.0×10^{-3} M acetone.

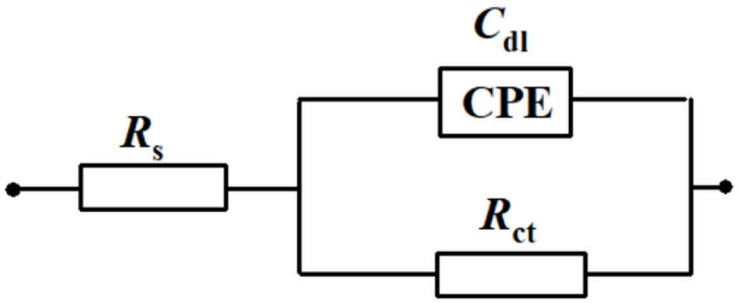

Figure 5. An equivalent circuit used to fit the recorded impedance data for the HER and OER processes, where R_{ct} and C_{dl} refer to the charge-transfer resistance and the double-layer capacitance (CPE-adjusted), linked in series with R_s—unbalanced solution resistance.

Table 1. Kinetic and interfacial properties derived from equivalent circuit modelling (Figure 5) of the HER on the Ni foam working electrode in 0.1 M NaOH. The listed charge-transfer resistance and double-layer capacitance metrics compare the pristine electrolyte against solutions modified with various acetone concentrations (the CPE exponents (φ) ranged between 0.69 and 0.91; $\chi^2 = 1.5 \times 10^{-5}$–$7.2 \times 10^{-4}$).

E/mV	R_{ct}/Ω g	C_{dl}/μF g^{-1}
0.1 M NaOH		
−50	6.67 ± 0.18	22,126 ± 590
−100	3.81 ± 0.09	19,887 ± 520
−150	2.91 ± 0.03	17,991 ± 417
−200	1.44 ± 0.01	13,294 ± 374
−250	0.58 ± 0.01	9880 ± 578
−300	0.27 ± 0.00	9530 ± 865
−350	0.17 ± 0.00	12,549 ± 1400
−400	0.12 ± 0.00	13,503 ± 1547
−450	0.10 ± 0.00	23,414 ± 3000
−500	0.08 ± 0.00	20,753 ± 2626
0.1 M NaOH + 10^{-5} M acetone		
−50	5.44 ± 0.21	38,405 ± 1390
−100	3.40 ± 0.07	35,808 ± 1002
−150	2.10 ± 0.02	24,666 ± 484
−200	0.87 ± 0.00	14,436 ± 305
−250	0.36 ± 0.00	8640 ± 515
−300	0.21 ± 0.00	7395 ± 673
−350	0.15 ± 0.00	8138 ± 865
−400	0.11 ± 0.00	7245 ± 713
−450	0.09 ± 0.00	10,521 ± 1365
−500	0.07 ± 0.00	6112 ± 787
0.1 M NaOH + 10^{-3} M acetone		
−50	5.88 ± 0.19	48,137 ± 1405
−100	3.47 ± 0.05	38,522 ± 653
−150	2.06 ± 0.01	23,852 ± 235
−200	0.84 ± 0.00	13,890 ± 326
−250	0.38 ± 0.00	9202 ± 587
−300	0.24 ± 0.00	10,721 ± 884
−350	0.16 ± 0.00	9135 ± 894
−400	0.13 ± 0.00	12,692 ± 1232
−450	0.10 ± 0.00	11,773 ± 1371
−500	0.09 ± 0.00	10,564 ± 1282

Table 1. *Cont.*

E/mV	R_{ct}/Ω g	C_{dl}/μF g^{-1}
0.1 M NaOH + 0.1 M acetone		
−100	41.57 ± 0.70	32,154 ± 210
−150	21.93 ± 0.23	30,699 ± 158
−200	12.56 ± 0.14	28,162 ± 207
−250	9.55 ± 0.12	23,864 ± 230
−300	7.10 ± 0.06	18,084 ± 180

Table 2. Kinetic and interfacial properties derived from equivalent circuit modelling (Figure 5) of the HER on the Ru-activated Ni foam working electrode in 0.1 M NaOH. The listed charge-transfer resistance and double-layer capacitance metrics compare the pristine electrolyte with solutions modified with varied acetone concentrations (the CPE exponents (φ) ranged between 0.72 and 0.90; $\chi^2 = 5.0 \times 10^{-6}$–$3.1 \times 10^{-4}$).

E/mV	R_{ct}/Ω g	C_{dl}/μF g^{-1}
0.1 M NaOH		
−50	0.36 ± 0.01	109,163 ± 4629
−100	0.24 ± 0.00	47,753 ± 766
−150	0.18 ± 0.00	31,867 ± 871
−200	0.14 ± 0.00	28,507 ± 852
−250	0.12 ± 0.00	26,052 ± 1199
−300	0.10 ± 0.00	25,451 ± 1245
−350	0.09 ± 0.00	27,205 ± 1576
−400	0.08 ± 0.00	28,459 ± 1266
−450	0.07 ± 0.00	35,195 ± 2911
−500	0.06 ± 0.00	29,547 ± 1647
0.1 M NaOH + 10^{-5} M acetone		
−50	5.34 ± 0.07	35,692 ± 428
−100	2.51 ± 0.03	30,453 ± 531
−150	1.71 ± 0.01	21,308 ± 230
−200	0.89 ± 0.00	14,698 ± 241
−250	0.42 ± 0.00	9974 ± 384
−300	0.24 ± 0.00	9760 ± 530
−350	0.16 ± 0.00	8996 ± 669
−400	0.12 ± 0.00	11,250 ± 898
−450	0.10 ± 0.00	10,529 ± 981
−500	0.08 ± 0.00	13,254 ± 1337
0.1 M NaOH + 10^{-3} M acetone		
−50	5.35 ± 0.09	42,000 ± 753
−100	3.44 ± 0.05	35,600 ± 664
−150	2.13 ± 0.01	25,706 ± 352
−200	0.95 ± 0.00	14,654 ± 268
−250	0.45 ± 0.00	10,732 ± 604
−300	0.26 ± 0.00	8954 ± 651
−350	0.20 ± 0.00	15,933 ± 1287
−400	0.15 ± 0.00	13,472 ± 989
−450	0.11 ± 0.00	12,785 ± 1158
−500	0.09 ± 0.00	10,978 ± 1027
0.1 M NaOH + 0.1 M acetone		
−100	9.81 ± 0.17	13,798 ± 246
−200	0.99 ± 0.00	9359 ± 137
−300	0.37 ± 0.00	5942 ± 259

Table 3. Temperature-dependent kinetic and interfacial properties (R_{ct} and C_{dl} parameters) derived from equivalent circuit modelling (Figure 5) of the HER on the Ni foam working electrode in 0.1 M NaOH (the CPE exponents (φ) ranged between 0.71 and 0.84; $\chi^2 = 4.0 \times 10^{-5}$–$4.7 \times 10^{-4}$).

E/mV	R_{ct}/Ω g				
	20 °C	**25 °C**	**30 °C**	**35 °C**	**40 °C**
−50	12.33 ± 0.12	2.33 ± 0.03	1.62 ± 0.03	1.20 ± 0.02	0.97 ± 0.02
−100	8.84 ± 0.09	2.15 ± 0.02	1.52 ± 0.01	1.14 ± 0.01	0.93 ± 0.01
−150	5.14 ± 0.06	2.06 ± 0.01	1.28 ± 0.01	0.92 ± 0.00	0.77 ± 0.00
−200	2.34 ± 0.01	1.24 ± 0.00	0.75 ± 0.00	0.54 ± 0.00	0.46 ± 0.00
−250	0.96 ± 0.00	0.58 ± 0.00	0.37 ± 0.00	0.28 ± 0.00	0.25 ± 0.00
−300	0.45 ± 0.00	0.31 ± 0.00	0.20 ± 0.00	0.17 ± 0.00	0.15 ± 0.00
	C_{dl}/μF g^{-1}				
−50	58,782 ± 429	53,768 ± 883	58,353 ± 1708	57,182 ± 1755	61,090 ± 2147
−100	53,472 ± 519	45,698 ± 660	45,563 ± 894	44,160 ± 1014	41,183 ± 903
−150	43,957 ± 563	39,125 ± 594	37,728 ± 967	34,547 ± 549	34,166 ± 444
−200	33,356 ± 312	30,905 ± 322	27,905 ± 571	26,751 ± 598	26,420 ± 544
−250	21,208 ± 451	22,049 ± 603	23,423 ± 831	22,250 ± 860	22,838 ± 852
−300	19,337 ± 869	23,598 ± 1051	18,907 ± 863	21,498 ± 1406	20,855 ± 1199

Table 4. Temperature-dependent kinetic and interfacial properties (R_{ct} and C_{dl} parameters) derived from equivalent circuit modelling (Figure 5) of the HER on the Ni foam working electrode in 0.1 M NaOH containing 1.0×10^{-3} M acetone (the CPE exponents (φ) ranged between 0.66 and 0.88; $\chi^2 = 1.7 \times 10^{-5}$–$4.4 \times 10^{-4}$).

E/mV	R_{ct}/Ω g				
	20 °C	**25 °C**	**30 °C**	**35 °C**	**40 °C**
−50	3.28 ± 0.08	2.38 ± 0.05	1.76 ± 0.05	1.31 ± 0.03	1.00 ± 0.02
−100	2.51 ± 0.04	2.02 ± 0.03	1.63 ± 0.02	1.25 ± 0.01	0.92 ± 0.01
−150	2.11 ± 0.02	1.68 ± 0.01	1.32 ± 0.01	0.95 ± 0.00	0.71 ± 0.00
−200	1.03 ± 0.00	0.95 ± 0.00	0.72 ± 0.00	0.54 ± 0.00	0.41 ± 0.00
−250	0.50 ± 0.01	0.44 ± 0.00	0.35 ± 0.00	0.28 ± 0.00	0.23 ± 0.00
−300	0.28 ± 0.00	0.22 ± 0.00	0.19 ± 0.00	0.16 ± 0.00	0.14 ± 0.00
	C_{dl}/μF g^{-1}				
−50	67,873 ± 1758	64,357 ± 1664	63,412 ± 2240	62,282 ± 1963	57,936 ± 1706
−100	47,817 ± 1048	44,731 ± 803	46,739 ± 1192	46,626 ± 1116	40,834 ± 730
−150	40,936 ± 863	38,092 ± 605	37,461 ± 526	35,485 ± 545	32,362 ± 323
−200	27,530 ± 362	28,481 ± 303	27,927 ± 581	26,524 ± 514	24,663 ± 353
−250	25,496 ± 1173	21,287 ± 501	21,253 ± 653	21,754 ± 769	22,371 ± 657
−300	26,427 ± 1248	16,620 ± 767	17,585 ± 801	16,383 ± 894	19,249 ± 1189

Hence, for the cathodically pre-treated Ni foam electrode, the recorded R_{ct} parameter declined from 6.67 Ω g at −50 mV to 1.44 Ω g at −200 mV and 0.08 Ω g at the electrode potential of −500 mV/RHE. Moderate concentrations of acetone in the working electrolyte significantly facilitated the charge-transfer resistance parameter, which substantially reduced at the initial and intermediate overpotentials, over the potential range characteristic to the activation reaction control. Hence, at the overpotentials of 50 and 200 mV, the R_{ct} came to 5.44 and 0.87 Ω g and 5.88 and 0.84 Ω g for the acetone concentrations of 1.0×10^{-5} and 1.0×10^{-3} M (see Table 1 for details). Then, fundamentally increasing values of the reaction resistance were recorded at the highest acetone concentration of 0.1 M, namely 41.57 and 7.10 Ω g, respectively, at the electrode potentials of −100 and −300 mV. This effect is most likely connected with expanded co-adsorption of ketone

molecules on the catalyst's surface. As previously argued in our earlier alkaline water electrolysis works [15,16], the introduction of acetone into sodium hydroxide solution resulted in significant facilitation of the rates of both H_2 and O_2 gas evolution processes on polycrystalline Ni and Pt electrode surfaces, respectively. The above is also fulfilled in current work and can be explained in terms of substantially diminished surface tension, resulting from interspecies hydrogen bonding between acetone and water. These effects could considerably promote the detachment of hydrogen (and oxygen for the OER) bubbles from the nickel foam electrode surface.

Simultaneously, a general trend for the recorded C_{dl} parameter was its continuous reduction along with rising cathodic polarisation (Table 1). This effect can be attributed to the partial shielding of the electrochemically active 3D Ni foam surface by freshly evolved hydrogen gaseous aggregates. Interestingly, after introduction of acetone into the electrolyte, the recorded C_{dl} parameter values started significantly rising. This effect is driven by several important factors, namely the above-mentioned facilitation of gas bubble detachment, the high polarizability of acetone molecules at the electrode/electrolyte interface, and improvement of the 3D surface wetting effect, allowing the electrolyte to thoroughly penetrate the interior pores of the nickel foam entity [22].

Moreover, the HER impedance behaviour for the Ru-activated nickel foam electrode, under similar experimental conditions, is shown in Figure 4 and Table 2. First of all, the significant Ni foam surface modification by Ru activation caused (understandably) a radical increase in the double-layer capacitance parameter for acetone-free sodium hydroxide solution (compare the corresponding C_{dl} values in Table 1 with those reported in Table 2). Also, the recorded values of the charge-transfer resistance at initial electrode overpotentials (activation reaction control) exhibited a radical reduction in the presence of ruthenium (compare 0.36 with 6.67 Ω g at −50 mV and 0.14 with 1.44 Ω g, recorded at −200 mV vs. RHE, respectively).

Then, the introduction of acetone at the concentration of 1.0×10^{-5} M dramatically slowed down the HER rates at the ruthenium-modified Ni foam electrode surface, where the recorded R_{ct} values came to 5.34 Ω g (at −50 mV) and 0.89 Ω g (at −200 mV). Also, the C_{dl} parameter exhibited a radical reduction at all studied electrode potentials. It should be noted that analogous behaviour was also observed at higher concentrations of acetone (see Table 2 for details). This effect is in contrast to that previously observed on the polycrystalline Pt electrode surface [16], most likely a consequence of fundamentally different acetone adsorption configuration at Ru. Compared to platinum, ruthenium is highly oxophilic and its surface has a strong affinity for both carbon and oxygen atoms. As a result, acetone molecules tend to become adsorbed on the Ru surface in a flat or side-on geometry (see Scheme 1 below), thus resulting in physical blocking of several ruthenium atoms (a steric effect) by a single acetone molecule [23,24].

Furthermore, the temperature-dependence (20–40 °C) of the HER process, examined in 0.1 M sodium hydroxide on the surface of the Ni foam electrode, both in the absence and presence of $(CH_3)_2C{=}O$, at the concentration of 1.0×10^{-3} M, is shown in Tables 3 and 4, respectively. Thus, as expected, the R_{ct} parameter exhibited significant temperature-dependent reduction with increasing electrolyte temperature over the entire examined overpotential range. Also, a rising temperature should generally lead to augmentation of the recorded double-layer capacitance values, but this expected effect is significantly hindered by an intensified hydrogen evolution reaction and thus extended Ni foam surface blockage by H_2 bubbles.

In the presence of acetone (Table 4), similar temperature dependence for the charge-transfer resistance and the double-layer capacitance parameters was observed. However, acetone-driven facilitation of the HER rates was limited to only the first two initial values

of temperature, which implies that adsorption of acetone molecules at temperatures above room temperature is very limited.

3.2.2. Oxygen Evolution Reaction

For the oxygen evolution reaction, the impedance measurements on the Ni foam/Ru-activated nickel foam electrodes were carried out over the potential range of 1500 through 2000 mV vs. RHE. The recorded Nyquist impedance plots also featured single and somewhat deformed semicircles at all examined potential values (see examples in Figures 6 and 7 below). Thus, for the unmodified Ni foam electrode and pure 0.1 M NaOH electrolyte, the recorded R_{ct} parameter diminished from 1.51 Ω g (at 1500 mV) to 0.08 Ω g (at 2000 mV). Then, the introduction of acetone resulted in a significant reduction in the R_{ct} parameter values recorded at 1500 mV to reach 1.18, 1.08 and 0.11 Ω g, respectively, for the ketone concentrations of 1.0×10^{-5}, 1.0×10^{-3} and 0.1 M (Table 5). Simultaneously, continuous Ni foam surface electrooxidation revealed radically increased double-layer capacitance values, with a rising tendency in the presence of acetone (compare the C_{dl} results presented in Table 5 with those of Table 1; also, refer to paragraph 3.2.1., pp. 5–6).

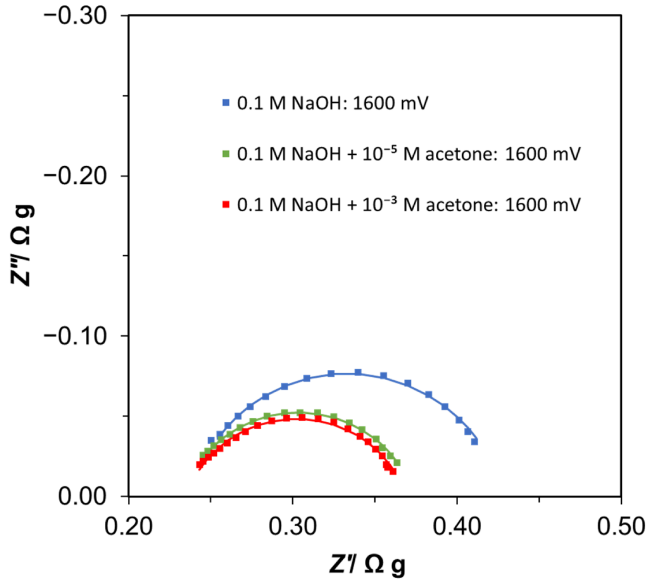

Figure 6. Impedance spectroscopy response (Nyquist curves) of the nickel foam working electrode during the oxygen evolution reaction. Data were gathered at a constant potential of 1600 mV in a blank 0.1 M NaOH background electrolyte and compared to solutions containing 1.0×10^{-5} M and 1.0×10^{-3} M acetone.

Table 5. Kinetic and interfacial properties derived from equivalent circuit modelling (Figure 5) of the OER on the Ni foam working electrode in 0.1 M NaOH. The listed charge-transfer resistance and double-layer capacitance metrics compare the pristine electrolyte with solutions modified with varied acetone concentrations (the CPE exponents (φ) ranged between 0.56 and 0.90; $\chi^2 = 4.2 \times 10^{-6}$–$1.2 \times 10^{-4}$).

E/mV	R_{ct}/Ω g	C_{dl}/μF g^{-1}
	0.1 M NaOH	
1500	1.51 ± 0.01	175,834 ± 1201
1600	0.19 ± 0.00	161,292 ± 3911
1700	0.11 ± 0.00	166,743 ± 9012
1800	0.10 ± 0.00	141,894 ± 10,260
1900	0.09 ± 0.00	170,929 ± 11,765
2000	0.08 ± 0.00	198,274 ± 13,615

Table 5. *Cont.*

E/mV	R_{ct}/Ω g	C_{dl}/μF g^{-1}
0.1 M NaOH + 10^{-5} M acetone		
1500	1.18 ± 0.01	341,991 ± 2358
1600	0.14 ± 0.00	338,827 ± 9953
1700	0.09 ± 0.00	500,000 ± 32,487
1800	0.08 ± 0.00	597,323 ± 37,956
1900	0.08 ± 0.00	462,522 ± 29,259
2000	0.07 ± 0.00	523,451 ± 38,237
0.1 M NaOH + 10^{-3} M acetone		
1500	1.08 ± 0.01	442,699 ± 4330
1600	0.13 ± 0.00	434,912 ± 11,250
1700	0.08 ± 0.00	606,726 ± 28,533
1800	0.07 ± 0.00	799,469 ± 42,962
1900	0.07 ± 0.00	572,434 ± 25,343
2000	0.07 ± 0.00	591,549 ± 32,942
0.1 M NaOH + 0.1 M acetone		
1500	0.11 ± 0.00	573,652 ± 33,504
1600	0.09 ± 0.00	479,014 ± 19,319
1700	0.07 ± 0.00	554,609 ± 39,452
1800	0.07 ± 0.00	441,710 ± 25,208
1900	0.06 ± 0.00	390,986 ± 34,446
2000	0.06 ± 0.00	492,609 ± 35,881

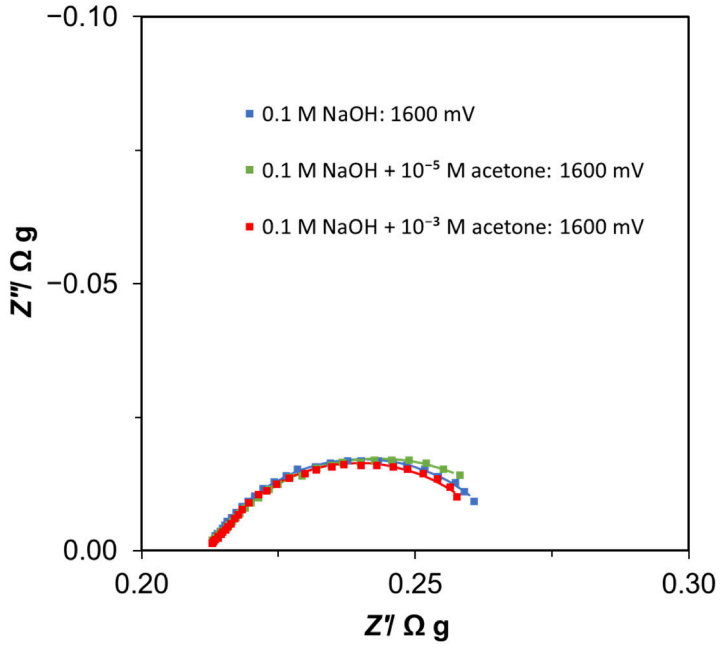

Figure 7. Impedance spectroscopy response (Nyquist curves) of the Ru-activated nickel foam working electrode during the oxygen evolution reaction. Data were gathered at a constant potential of 1600 mV in a blank 0.1 M NaOH background electrolyte and in solutions containing 1.0 × 10^{-5} M and 1.0 × 10^{-3} M acetone.

Then, the OER impedance behaviour for the Ru-modified nickel foam electrode is shown in Figure 7 and Table 6. Again, the presence of ruthenium particles (in their oxide form) led to a radical facilitation of the OER kinetics, where the recorded R_{ct} parameter values came to 0.08 and 0.04 Ω g at the electrode potentials of 1500 and 2000 mV vs. RHE,

respectively. Also, the presence of ruthenium resulted in a significant rise in the recorded C_{dl} values (compare the reported resistance and interfacial capacitance values in the absence of acetone in Tables 5 and 6). However, as can be seen in Table 6, the introduction of acetone (irrespective of its concentration) had practically no catalytic effect on the recorded OER rates. The above could be explained in terms of acetone molecules being unable to form stable bonding on the electrooxidized Ru-activated nickel foam electrode surface under continuous oxygen evolution [25].

Table 6. Kinetic and interfacial properties derived from equivalent circuit modelling (Figure 5) of the OER on the Ru-activated Ni foam working electrode in 0.1 M NaOH. The listed charge-transfer resistance and double-layer capacitance metrics compare the pristine electrolyte against solutions modified with varied acetone concentrations (the CPE exponents (φ) ranged between 0.64 and 0.90; $\chi^2 = 1.4 \times 10^{-6}$–$1.5 \times 10^{-5}$).

E/mV	R_{ct}/Ω g	C_{dl}/μF g^{-1}
0.1 M NaOH		
1500	0.08 ± 0.00	496,076 ± 21,412
1600	0.06 ± 0.00	376,640 ± 10,245
1700	0.05 ± 0.00	304,970 ± 14,726
1800	0.04 ± 0.00	270,785 ± 14,283
1900	0.04 ± 0.00	264,668 ± 15,843
2000	0.04 ± 0.00	325,453 ± 20,075
0.1 M NaOH + 10^{-5} M acetone		
1500	0.08 ± 0.00	378,712 ± 9716
1600	0.06 ± 0.00	536,942 ± 17,360
1700	0.04 ± 0.00	265,755 ± 13,185
1800	0.04 ± 0.00	242,495 ± 13,379
1900	0.03 ± 0.00	238,028 ± 18,693
2000	0.03 ± 0.00	252,777 ± 20,714
0.1 M NaOH + 10^{-3} M acetone		
1500	0.07 ± 0.00	409,960 ± 14,464
1600	0.05 ± 0.00	388,350 ± 11,448
1700	0.04 ± 0.00	213,803 ± 11,384
1800	0.04 ± 0.00	183,962 ± 10,260
1900	0.03 ± 0.00	181,471 ± 14,087
2000	0.03 ± 0.00	201,408 ± 12,565

3.3. Steady-State Tafel Polarisation Curves

Figures 8–11 present quasi-potentiostatic, cathodic (HER) and anodic (OER) Tafel polarisation plots, recorded on the nickel foam and the Ru-activated Ni foam electrodes, in pure 0.1 M NaOH solution and in the presence of acetone, at the concentrations of 1.0×10^{-5}, 1.0×10^{-3} and 0.1 M. Hence, it can be seen in Figure 8 that the introduction of acetone (especially at the two initial ketone concentrations) into alkaline electrolyte caused a significant reduction in the recorded cathodic Tafel slopes (b_c), which also coincides with considerably increased current densities at the overpotential range of 200–300 mV. Most importantly, at the concentration of 0.1 M, acetone severely impeded the HER rates, which is also reflected in a radically reduced exchange current-density parameter (ca. 2 orders of magnitude, as compared to the acetone-free solution). These results are totally in line with the *ac.* impedance data presented in Table 1.

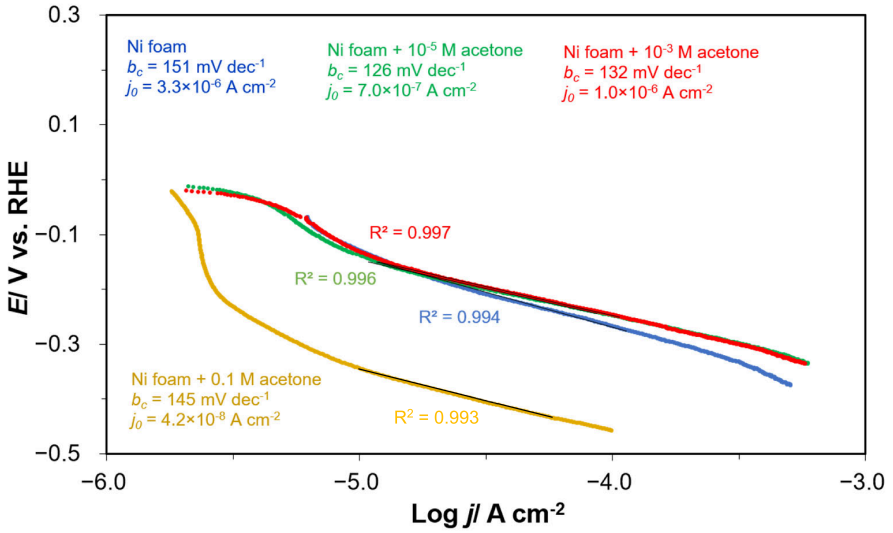

Figure 8. The influence of acetone concentration on the cathodic Tafel polarisation of the nickel foam working electrode in 0.1 M NaOH. Data were collected quasi-potentiostatically at a scan rate of 0.5 mV s^{-1}. Ohmic drop (*iR*) compensation was applied using solution resistance values determined via impedance spectroscopy.

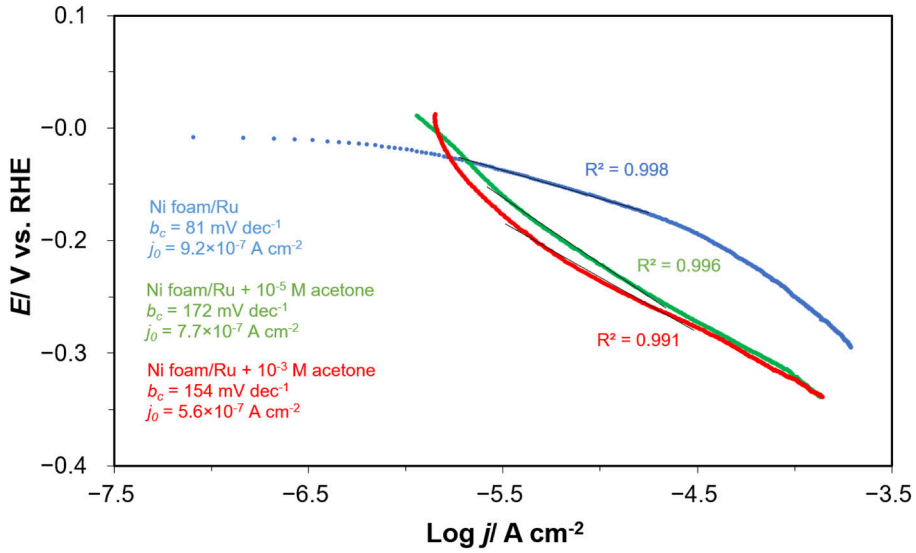

Figure 9. The influence of acetone concentration on the cathodic Tafel polarisation of the Ru-modified nickel foam working electrode in 0.1 M NaOH. Data were collected quasi-potentiostatically at a scan rate of 0.5 mV s^{-1}. Ohmic drop (*iR*) compensation was applied using solution resistance values determined via impedance spectroscopy.

In addition, for the Ru-activated nickel foam electrode, the presence of acetone resulted in significant deterioration of the HER kinetics (Figure 9), which is reflected in both radically rising cathodic Tafel slopes (from 81 to 172 and 154 mV dec^{-1}, respectively, for the ketone-free, 1.0 × 10^{-5} M and 1.0 × 10^{-3} M acetone concentrations) and decreasing values of the exchange current-density (see Figure 9, also compare with the impedance results presented in Table 2). However, it should be noted that the current-density data for the polarisation plots were calculated based on the surface-area estimations from the double-layer capacitance measurements, carried out at the HER overpotential of 50 mV. Here, an assumption was made that a commonly used value of 20 μF cm^{-2} is used in the scientific literature for smooth and homogeneous surfaces (see Reference [3] and other papers referred there). Hence, the estimated electrochemically active surface area came to

about 50 cm^2 (m_s = 45.2 mg) and 271 cm^2 (m_s = 49.7 mg) for the unmodified Ni foam and the Ru-activated nickel foam electrodes, respectively.

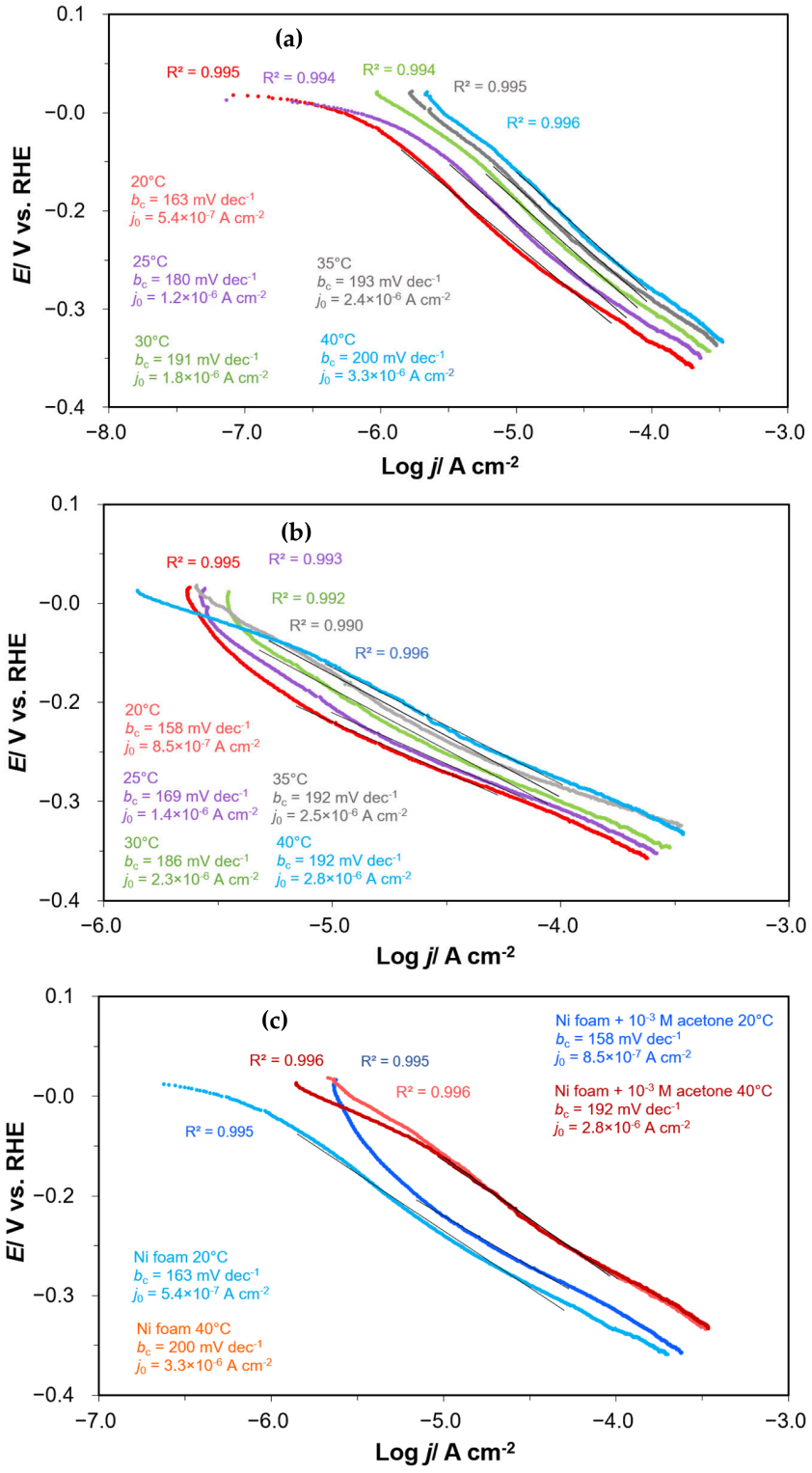

Figure 10. (**a**) Temperature-dependent cathodic Tafel polarisation curves of the nickel foam working electrode in 0.1 M NaOH. Data were collected quasi-potentiostatically at a scan rate of 0.5 mV s^{-1}. Ohmic drop (*iR*) compensation was applied using solution resistance values determined via impedance spectroscopy; (**b**) as in (**a**) above, but obtained in the presence of 1.0 × 10^{-3} M acetone; (**c**) as in (**a**,**b**) above, but comparison was made between the 20 and 40 °C results, in the absence and presence of acetone.

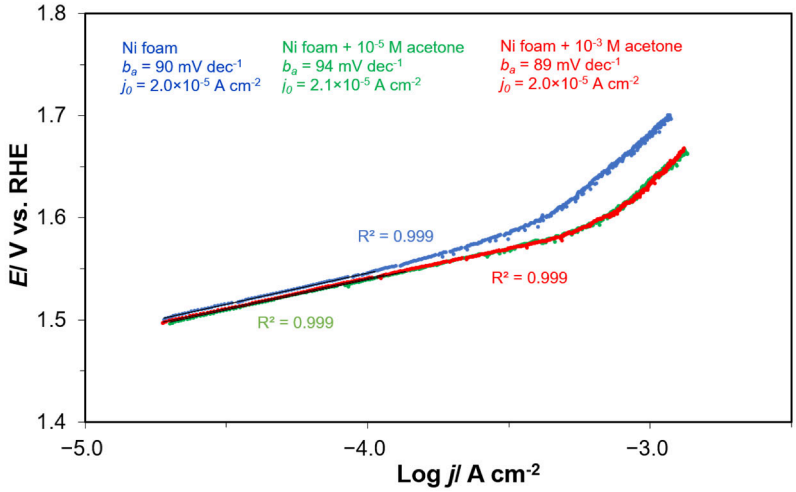

Figure 11. The influence of acetone concentration on the anodic Tafel polarisation of the nickel foam working electrode in 0.1 M NaOH. Data were collected quasi-potentiostatically at a scan rate of 0.5 mV s^{-1}. Ohmic drop (*iR*) compensation was applied using solution resistance values determined via impedance spectroscopy.

Although a proper electrochemical assessment of complex 3D electrode structures is always a very difficult matter, the undertaken approach allowed for partial, qualitative extraction of the surface area increase from the catalytic properties of the surface–Ru particles modifier (compare the recorded b_c and j_0 parameter values for the unmodified and the ruthenium-activated Ni foam electrodes in Figures 8 and 9 with those reported in Reference [3]).

Figure 10 below presents temperature-dependent (20–40 °C) cathodic Tafel polarisation plots, recorded on the unmodified nickel foam electrode in 0.1 M NaOH solution, in the absence (Figure 10a) and presence of 1.0 × 10^{-3} M acetone (Figure 10b). Hence, the temperature rise from 20 to 40 °C resulted in the b_c parameter rising from 163 mV dec^{-1} (at 20 °C) to reach 200 mV dec^{-1} (at 40 °C). At the same time, the j_0 parameter exhibited significant facilitation from 5.4 × 10^{-7} A cm^{-2} (at 20 °C) to 3.3 × 10^{-6} A cm^{-2} (at 40 °C). An analogous situation was recorded in the presence of acetone, where the b_c and j_0 parameters increased from 158 mV dec^{-1} and 8.5 × 10^{-7} A cm^{-2} (at 20 °C) to 192 mV dec^{-1} and 2.8 × 10^{-6} A cm^{-2} (at 40 °C). The influence of acetone on the HER kinetics at the two temperature extremes is shown in Figure 10c (please note that the effect of acetone at 40 °C is rather insignificant). It should be stressed, however, that obtaining higher HER rates at lower temperatures is definitely beneficial from the corrosion performance point of view.

Finally, Figure 11 presents anodic polarisation plots, recorded on the nickel foam electrode in 0.1 M NaOH solution, in the absence and presence of acetone, at the concentrations of 1.0 × 10^{-5} and 1.0 × 10^{-3} M. Although all recorded b_c and j_0 parameters came to approximately 90 mV dec^{-1} and 2.0 × 10^{-5} A cm^{-2} (as derived for the low anodic overpotential range), for electrode potentials exceeding 1.55 V/RHE, the influence of acetone on the OER rates became substantial (Figure 11). This effect is entirely in line with the former impedance spectroscopy findings (also refer to the j_0 values reported on a similar experimental system in References [26–28]).

4. Conclusions

Acetone, at moderate concentrations, was found to considerably facilitate the kinetics of both the HER and the OER processes on the nickel foam electrode in sodium hydroxide solution. However, the presence of acetone in the electrolyte for the Ru-activated nickel

foam electrode resulted in a radical deceleration of the HER rates. This is strongly believed to be associated with the electrode surface poisoning effect, in relation to the blockage of the ruthenium sites by an extensive side-on coordination of adsorbed acetone molecules. As expected, an increased reaction temperature resulted in facilitation of the HER kinetics on the Ni foam electrode surface, but the effect of acetone at 40 °C was already negligible (most likely due to very limited ketone adsorption under these experimental conditions). Nevertheless, attaining higher HER rates at lower temperatures might sound advantageous from a materials durability perspective.

Finally, the presence of acetone had practically no effect on the recorded OER rates on the ruthenium-modified nickel foam electrode. This could be explained in terms of acetone molecules being unable to form durable binding on the electrooxidized, ruthenium-modified nickel foam electrode surface during uninterrupted oxygen evolution.

These conclusions indicate that some organic additives, such as acetone, might exhibit significant, although strongly catalyst-dependent, opportunities for the facilitation of the industrial alkaline water electrolysis process. However, further examinations of this process are necessary to be carried out in order to fully explain the mechanism of acetone electrosorption on the nickel (ruthenium-modified nickel) foam surface and its further (concentration-dependent) interaction with the hydrogen and oxygen evolution processes.

Author Contributions: B.P. was a scientific initiator and work coordinator who wrote this manuscript; J.K. ran the experiments under the supervision of B.P. and carried out treatment of all the results. All authors have read and agreed to the published version of the manuscript.

Funding: This work has primarily been financed by internal research grant no. 30.610.001-110, provided by the University of Warmia and Mazury in Olsztyn.

Institutional Review Board Statement: Not applicable.

Informed Consent Statement: Not applicable.

Data Availability Statement: Data supporting the reported results will be available upon request.

Conflicts of Interest: The authors declare no conflicts of interest.

References

1. Xu, X.; Shao, Z.; Jiang, S.P. High-Entropy Materials for Water Electrolysis. *Energy Technol.* **2022**, *10*, 2200573. [CrossRef]
2. Hussain, T.; Truong, L.; Hussain, S.; Patil, S.A.; Chun, S.H.; Kaseem, M. Novel core-shell structured electro-catalyst with 1D-$NiTe_2$ over 3D metal structure for efficient hydrogen evolution reactions. *J. Alloys Compd.* **2022**, *918*, 165797. [CrossRef]
3. Pierozynski, B.; Mikolajczyk, T.; Kowalski, I.M. Hydrogen evolution at catalytically-modified nickel foam in alkaline solution. *J. Power Sources* **2014**, *271*, 231–238. [CrossRef]
4. Becker, H.; Murawski, J.; Shinde, D.V.; Stephens, I.E.L.; Hinds, G.; Smith, G. Impact of Impurities on Water Electrolysis: A Review. *Sustain. Energy Fuels* **2023**, *7*, 1565–1603. [CrossRef]
5. Barwe, S.; Mei, B.; Masa, J.; Schuhmann, W.; Ventosa, E. Overcoming Cathode Poisoning from Electrolyte Impurities in Alkaline Electrolysis by Means of Self-Healing Electrocatalyst Films. *Nano Energy* **2018**, *53*, 763–768. [CrossRef]
6. Howard, K.S.; McAllister, R.A. Surface Tension of Acetone-water Solutions Up to Their Normal Boiling Points. *AIChE J.* **1957**, *3*, 325–329. [CrossRef]
7. Wu, N.; Li, X.; Liu, S.; Zhang, M.; Ouyang, S. Effect of Hydrogen Bonding on the Surface Tension Properties of Binary Mixture (Acetone-Water) by Raman Spectroscopy. *Appl. Sci.* **2019**, *9*, 1235. [CrossRef]
8. Shah, S.K.; Bhattarai, G.; Bhattarai, A. Acetone as a Modulator of Surfactant Behavior in Mixed Solvents: Surface Tension, Viscosity, and Micellization. *J. Nepal Chem. Soc.* **2025**, *45*, 39–47. [CrossRef]
9. Mekazni, D.S.; Arán-Ais, R.M.; Feliu, J.M.; Herrero, E. Understanding the electrochemical hydrogenation of acetone on Pt single crystal electrodes. *J. Electroanal. Chem.* **2022**, *922*, 116697. [CrossRef]
10. Bondue, C.J.; Koper, M.T.M. A mechanistic investigation on the electrocatalytic reduction of aliphatic ketones at platinum. *J. Catal.* **2019**, *369*, 302–311. [CrossRef]
11. Bondue, C.J.; Liang, Z.; Koper, M.T.M. Dissociative Adsorption of Acetone on Platinum Single-Crystal Electrodes. *J. Phys. Chem. C* **2021**, *125*, 6643–6649. [CrossRef] [PubMed]

12. Bondue, C.J.; Koper, M.T.M. Electrochemical Reduction of the Carbonyl Functional Group: The Importance of Adsorption Geometry, Molecular Structure, and Electrode Surface Structure. *J. Am. Chem. Soc.* **2019**, *141*, 12071–12078. [CrossRef] [PubMed]
13. Marth, A.; Piehler, J.; Brodt, M.; Maier, M.; Thiele, S. Investigation of the Electrocatalytic reduction of simple ketones in alkaline media. *Electrochem. Commun.* **2025**, *172*, 107880. [CrossRef]
14. Liu, Y.; Zeng, Y.; Liu, R.; Wu, H.; Wang, G.; Cao, D. Poisoning of acetone to Pt and Au electrodes for electrooxidation of 2-propanol in alkaline medium. *Electrochim. Acta* **2012**, *76*, 174–178. [CrossRef]
15. Kuczyński, M.; Mikołajczyk, T.; Pierożyński, B.; Pszczółkowski, B. Facilitation of the Kinetics of Alkaline Water Electrolysis on Polycrystalline Nickel Electrode by Introduction of Acetone to 0.1 M NaOH Working Solution. *Appl. Sci.* **2025**, *15*, 5949. [CrossRef]
16. Adamicka, A.; Mikołajczyk, T.; Kuczyński, M.; Pierożyński, B. The Influence of Acetone on the Kinetics of Water Electrolysis Examined at Polycrystalline Pt Electrode in Alkaline Solution. *Catalysts* **2024**, *14*, 488. [CrossRef]
17. Macdonald, J.R. *Impedance Spectroscopy, Emphasizing Solid Materials and Systems*; John Wiley & Sons: New York, NY, USA, 1987; pp. 1–368.
18. Alsabet, M.; Grdeń, M.; Jerkiewicz, G. Electrochemical Growth of Surface Oxides on Nickel. Part 3: Formation of β-NiOOH in Relation to the Polarization Potential, Polarization Time, and Temperature. *Electrocatalysis* **2015**, *6*, 60–71. [CrossRef]
19. Watson, N.I.; Keegan, M.; van den Bosch, B.; Yan, N.; Rothenberg, G. The Influence of Metal Impurities on NiOOH Electrocatalytic Activity in the Oxygen Evolution Reaction. *ChemElectroChem* **2024**, *11*, e202400223. [CrossRef]
20. Pajkossy, T. Impedance of rough capacitive electrodes. *J. Electroanal. Chem.* **1994**, *364*, 111–125. [CrossRef]
21. Schalenbach, M.; Durmus, Y.E.; Robinson, S.A.; Tempel, H.; Kungl, H.; Eichel, R.A. Physicochemical Mechanisms of the Double-Layer Capacitance Dispersion and Dynamics: An Impedance Analysis. *J. Phys. Chem. C* **2021**, *125*, 5870–5879. [CrossRef]
22. Lu, Y.M.; Hong, S.H. Preparation of Electrodes with β-Nickel Hydroxide/CVD-Graphene/3D-Nickel Foam Composite Structures to Enhance the Capacitance Characteristics of Supercapacitors. *Materials* **2024**, *17*, 23. [CrossRef] [PubMed]
23. Zhu, S.; Qin, X.; Xiao, F.; Yang, S.; Xu, Y.; Tan, Z.; Li, J.; Yan, J.; Chen, Q.; Chen, M.; et al. The role of ruthenium in improving the kinetics of hydrogen oxidation and evolution reactions of platinum. *Nat. Catal.* **2021**, *4*, 711–718. [CrossRef]
24. Avery, N.R.; Anton, A.B.; Toby, B.H.; Weinberg, W.H. Contrasting bonding configurations of acetone on Pt(111) and Ru(001) surfaces. *J. Electron Spectrosc. Relat. Phenom.* **1983**, *29*, 233–237. [CrossRef]
25. Jia, S.; Zhang, J.; Liu, Q.; Ma, C.; Tang, Y.; Sun, H. Competitive adsorption of oxygen-containing intermediates on ruthenium–tin solid-solution oxides for alkaline oxygen evolution. *J. Mater. Chem. A* **2023**, *11*, 23489–23497. [CrossRef]
26. Yang, X.; Zhang, W.; Huang, L. Enhancing oxygen evolution reaction performance of ultrasonically treated nickel electrodes in alkaline media. *Int. J. Electrochem. Sci.* **2025**, *20*, 100884. [CrossRef]
27. Foroughi, F.; Faid, A.Y.; Sunde, S.; Pollet, B.G. Sonoactivated polycrystalline Ni electrodes for alkaline oxygen evolution reaction. *Ultrason. Sonochem.* **2022**, *86*, 106013. [CrossRef] [PubMed]
28. Van der Heijden, O.; Park, S.; Eggebeen, J.J.J.; Koper, M.T.M. Non-Kinetic Effects Convolute Activity and Tafel Analysis for the Alkaline Oxygen Evolution Reaction on NiFeOOH Electrocatalysts. *Angew. Chem. Int. Ed.* **2023**, *62*, e202216477. [CrossRef] [PubMed]